Chapter 18
Influence of Printing Constraints on Residual Stresses of FDM Parts

C. Casavola, A. Cazzato, V. Moramarco, and G. Pappalettera

Abstract The Fused Deposition Modelling (FDM) is nowadays one of the most widespread and employed processes to build complex 3D prototypes directly from a STL model. In this technique, the part is built as a layer-by-layer deposition of a feedstock wire. This typology of deposition has many advantages but produces rapid heating and cooling cycles of the feedstock material that introduces residual stresses in the part during the build-up. Consequently, warping, de-layering and distortion of the part during the print process are common issues in FDM parts and are related to residual stresses. The common techniques employed to obtain parts of correct shape and dimensions, such as depositing glue on the bed, have the aim to constrain the object on the printing bed, though this increases the residual stresses in the parts. The aim of the present work is to measure the residual stresses in several points of printed parts, both on top and bottom, in order to verify if the constrain conditions used during the printing produce substantial variation from a point to another. The residual stresses have been measured in ABS parts employing the hole-drilling method. In order to avoid the local reinforcement of the strain gage, an optical technique, i.e. ESPI (electronic speckle pattern interferometry), is employed to measure the displacement of the surface due to the stress relaxation and, consequently, calculate the residual stresses.

Keywords 3D printing • Residual stress • Fused deposition modelling • Hole drilling • ESPI

18.1 Introduction

The Fused Deposition Modelling (FDM), invented in the early 1990s by Stratasys, is one of the most employed 3D printing techniques in both consumer and enterprise business. This process has been employed to build complex 3D prototypes directly from a computerized solid model in many fields such as aerospace, medical, construction, and cultural [1, 2] but, nowadays, there are many other potential fields where it can be employed. Moreover, the diffusion of the low-cost desktop 3D printers such as RepRap, Ultimaker, Maker-Bot, Cube, etc., has made this technology widely accessible even at home and office. In this process, as for many others 3D printing technologies [3], the model is built as a layer-by-layer deposition of a feedstock material. Initially, the raw material is in the form of a filament that is partially melted, extruded and deposited by a numerically controlled heated nozzle onto the previously built model [1]. After the deposition, the material cools, solidifies and sticks with the surrounding material. Due to the layer-by-layer construction and the orientation of the material deposition, once the entire model has been deposited, the FDM part shows orthotropic material properties with a behaviour similar to a laminate orthotropic structure [4]. Initially, the FDM printers have been able to build parts only in acrylonitrile-butadiene-styrene (ABS) and polylactic acid (PLA). However, nowadays, many others materials have been employed and developed, e.g., metal [5], ceramics [6], bioresorbable polymer (PCL) [7], metal/polymers mixture materials [8], and short fibre composites [9]. The PLA, compared to ABS, have a stronger mechanical resistance and a lower coefficient of thermal expansion. The last property improves the printability of the material because reduces the de-layering problems and the warp effect during the printing phase. This distortion effect of the part during the print is one of the most important issues in the FDM process, because it could seriously affect the shape and the final dimensions of the parts or it could prevent the finalization of the objects due to unsticking of the object from the bed. The distortions are due to the continuous rapid heating and cooling cycles of the deposited material [10, 11]. A common technique in order to reduce this problem is to employ a heated bed with some type of adhesive on the surface. Although, such procedures help to reduce distortions, they can increase the residual stresses of the final part.

C. Casavola • A. Cazzato • V. Moramarco (✉) • G. Pappalettera
Dipartimento di Meccanica, Matematica e Management (DMMM), Politecnico di Bari, Viale Japigia 182, 70126, Bari, Italy
e-mail: vincenzo.moramarco@poliba.it

A. Baldi et al. (eds.), *Residual Stress, Thermomechanics & Infrared Imaging, Hybrid Techniques and Inverse Problems, Volume 8*,
Conference Proceedings of the Society for Experimental Mechanics Series, DOI 10.1007/978-3-319-62899-8_18

Some papers have dealt with experimental measurements of residual stress distribution in plastic parts [12–14] but few works in FDM parts [11, 15]. Turnbull et al. [12] carried out a comparison among several techniques to measure residual stresses in ABS, Polycarbonate, and Nylon. They concluded that the hole drilling can be employed as a valid measurement method to measure residual stresses in plastic materials. Nau et al. [13] highlighted that the process parameters and procedures applied for stress analysis in metallic materials cannot be employed in polymers. They pointed out that the surface preparation of specimens, the strain gauge bonding, and the drilling speed are critical issues in order to obtain a correct measure. However, both Turnbull et al. [12] and Nau et al. [13] did not consider the local reinforcement effect that the installation of a rosette produces in materials that have a low Young's modulus. Indeed, Magnier et al. [14] studied the influence of material viscoelasticity, room temperature and local reinforcement of the strain gauge on the measure of deformation by HDM of plastic materials. They highlighted that the use of strain gauge to measure the deformation on plastic materials can produce a difference up to 30% between the results recorded by strain gauge and DIC. Casavola et al. [11, 16–17] studied the effect on residual stresses of the raster orientation in FDM parts. They found that the stacking sequence $+45°/-45°$ shows the lowest values of residual stresses. Moreover, they highlighted that there is not a clear difference between the bottom and the top of the printed specimens. Only one paper has tried to deal with the residual stress issues in FDM part by numerical simulation. Zhang and Chou [18], using simplified material properties and boundary conditions, have simulated different deposition patterns and have demonstrated the feasibility of using the element activation function to reproduce the filament deposition. They found that there was a modification of the residual stress distributions changing the tool-path pattern. However, they did not validate their model using residual stress measurements but only by comparing the distortion of the printed part and the numerical prediction.

The aim of the present work is to measure the residual stresses in several points of printed parts, both on top and bottom, in order to verify if the constrain conditions employed during the printing produce a substantial variation from a point to another. The residual stresses have been measured in ABS parts employing the hole-drilling method. In order to avoid the local reinforcement of the strain gage, an optical technique, i.e. ESPI (electronic speckle pattern interferometry), is employed to measure the displacement of the surface due to the stress relaxation and, consequently, to calculate the residual stresses.

18.2 Materials and Methods

A RepRap Prusa i3 equipped with a marlin firmware and a nozzle with a diameter of 0.4 mm has been employed to produce the specimens. These have a rectangular shape and the dimensions of $80 \times 40 \times 7$ mm. Four stacking sequences have been studied, i.e., the raster angles are $\pm 30°$, $\pm 45°$, $0°/90°$ and $0°$ only. A layer with a $0°$ raster angle has the deposited beads parallel to the major side of the specimen. Moreover, the samples have been manufactured with the minimum dimension of the part perpendicular to the build platform. The Fig. 18.1 shows the coordinate system for the deposition and for the residual stresses.

The parameters reported in Table 18.1, such as the layer thickness or the number of contour lines, have been kept constant for every specimen.

In Table 18.1, the air gap is the distance between two, adjacently deposited, beads of the same layer; the layer thickness and the bead width are respectively the height and the width of a deposited filament. The number of contours represents how many edges have been deposited before filling the inner part by inclined beads. The bed temperature has been set to 90 °C and some glue on the bed has been employed to reduce the warping effect. The solid model, created using a 3D CAD, has been sliced using the open source software Slic3r.

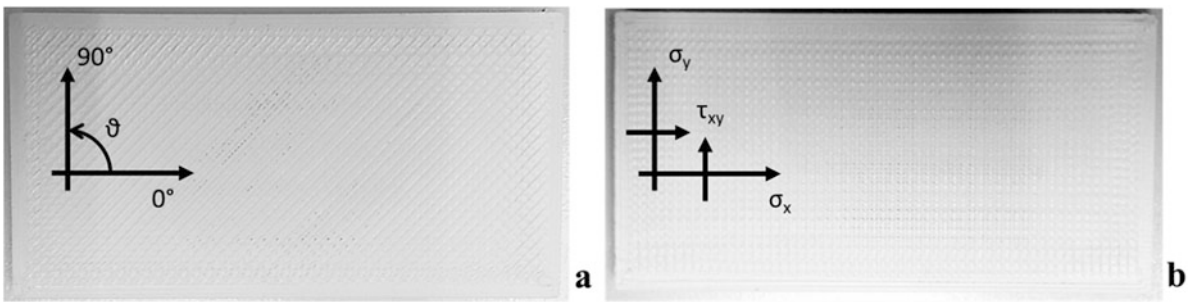

Fig. 18.1 Specimen examples with $\pm 45°$ (**a**) and $0°/90°$ (**b**) stacking sequence

Table 18.1 Fixed printer parameters

Parameter	Value
Air gap [mm]	0
Layer thickness [mm]	0.2
Bead width [mm]	0.67
Number of contour lines	3
Bed temperature [°C]	90
Nozzle temperature [°C]	215

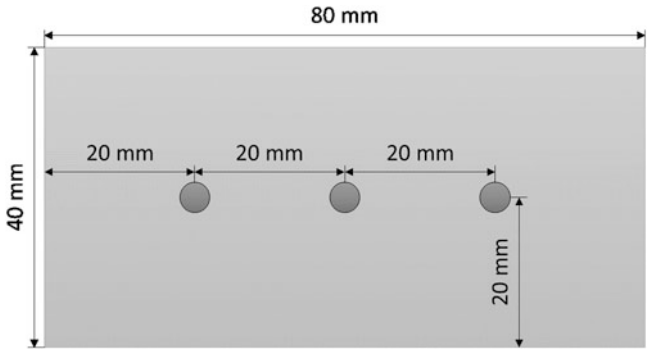

Fig. 18.2 Holes position on the *top* and the *bottom* of the specimens

In this work, the ESPI technique has been employed to measure the displacement around a hole drilled inside the material. Due to the orthotropic behaviour of FDM parts, the isotropic model usually implemented in commercial hole drilling software cannot be used. Thus, an orthotropic FEM model has been developed to calculate the displacements due to some known stress cases. The combination between the experimental displacement data and the FE model allows calculating the residual stress in the parts [17].

The measure of the residual stresses has been carried out on three different samples for each stacking sequence and in order to calculate the mean values. Moreover, three holes have been drilled on the top of each specimen, i.e. starting from the last layer deposited, and three on the bottom, i.e. starting from the first layer deposited (Fig. 18.2). Finally, an average value of the two side holes has been calculated and compared to the values of the central hole.

The holes were drilled by means of a high-speed turbine which is mounted on a precision travel stage. Turbine rotation speed was set to 5,000 rpm after some preliminary tests that indicated that this speed allows obtaining good quality holes [11]. The cutter is made by tungsten coated by TiN and it has a nominal diameter $d = 1.59$ mm. Compressed air was activated during the test to clean the surface of the sample by the formation of drilling chips. The holes were drilled to a depth of 0.6 mm through 30 drill increments to contain the temperature during the drilling phase on lower values. In order to reduce the computational time, the residual stress calculation has been done on 15 drill increments.

A diode pumped solid-state laser source ($\lambda = 532$ nm) was used to shine the sample and to generate the speckle pattern. The laser beam is divided in two parts by a beamsplitter and delivered by two optical fibres. The beam emerging out from the first fibre is collimated and then directed towards the sample at a given angle ($\alpha = 54°$). The beam emerging from the second fibre, instead, is directed towards the CCD matrix of the camera and it acts as a reference beam. The CCD camera (640×480 pixel) itself is placed at a given angle with respect to the normal to the sample ($\beta = 34°$). Light diffused by the sample interferes on the CCD matrix with the reference beam. Four-step temporal phase shifting algorithm was adopted in order to obtain the phase [19, 20]. This means that four reference images are taken initially having a $\pi/2$ phase difference among each other. Another set of four images is, analogously taken for each drill increment. These intensity patterns were subtracted from the reference intensity patterns recorded on the sample before starting the drilling procedure. This operation allows obtaining fringe patterns encoding the information about the displacement experienced by the sample along the sensitivity vector.

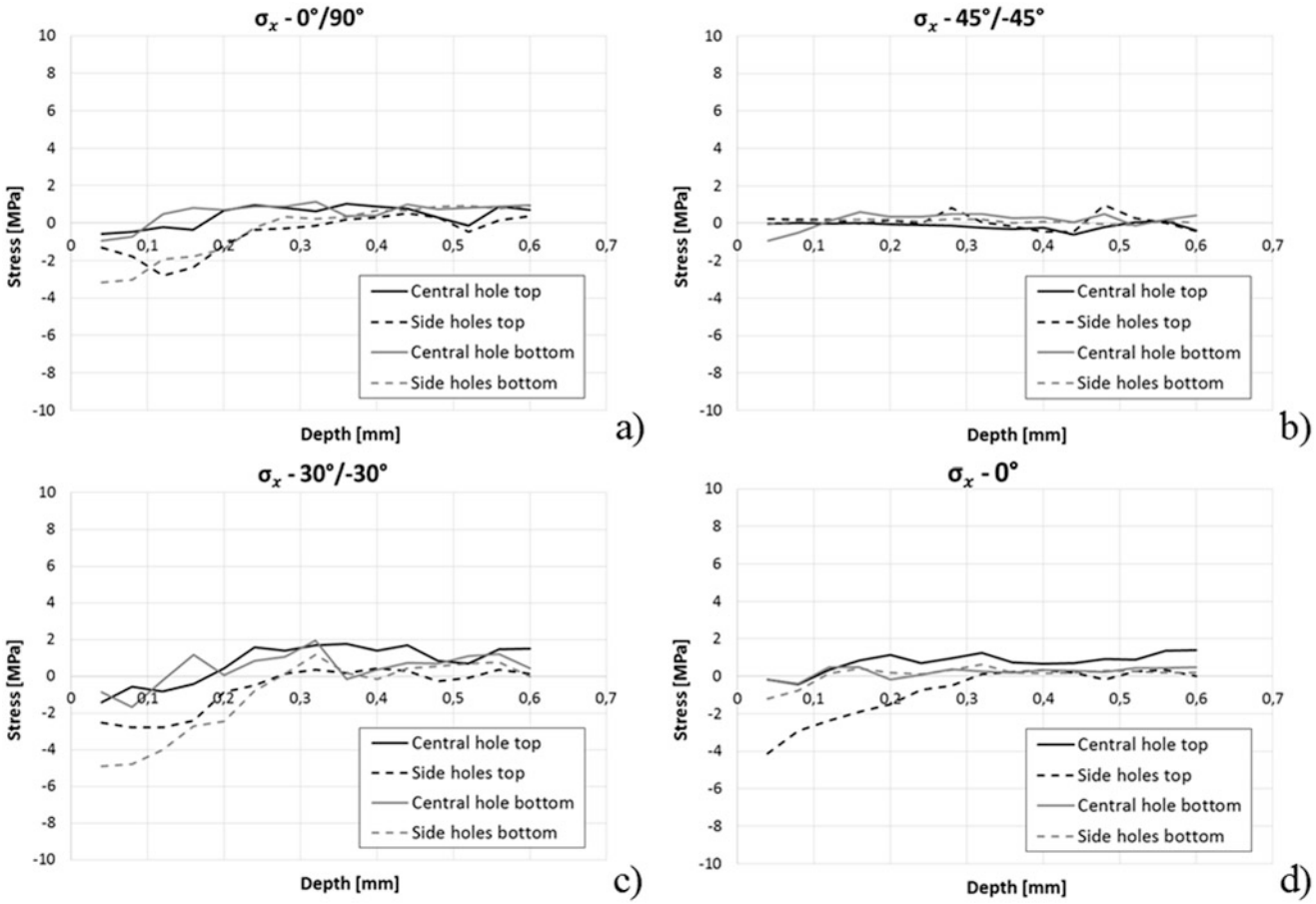

Fig. 18.3 Residual stresses in x direction for 0°/90° (**a**), 45°/−45° (**b**), 30°/−30° (**c**) and 0° (**d**) raster orientations

18.3 Results and Discussions

The σ_x, σ_y, and τ_{xy} residual stresses trends for the four stacking sequences and for the top and the bottom of the specimens have been shown in Figs. 18.3, 18.4 and 18.5. Moreover, it has been reported the comparison between the side holes and the central hole residual stresses values. As pointed out also by Casavola et al. [15], there are some differences among the studied configurations for σ_x and σ_y residual stresses. These differences are remarkable near the surface of the specimens, i.e. until 0.2 mm, while no clear differences can be identified in depth for all the stacking sequences. The ±30° configuration shows (Figs. 18.3c and 18.4c) the higher absolute values of residual stress both on the top and on the bottom of the specimens. Moreover, this stacking sequence shows the highest value of residual stress recorded during this experimental campaign (Fig. 18.4c).

The lowest residual stresses have been measured in ±45° in the specimens. Both in the σ_x and τ_{xy} are near the zero both on the top and on the bottom of the specimens (Figs. 18.3b and 18.5b), while the σ_y, although is not null, shows values lower in comparison with the other configurations (Fig. 18.4b).

The comparison between the residual stresses in side and central positions shows that, generally, the σ_x is higher in the side positions. The difference is remarkable near the surface and beyond 0.2 mm, while, in depth, the residual stresses tend to a value near zero. On the other hand, for the σ_y stress, the difference between the side and central holes is not clear and the trends are almost overlapped. The difference between side and central hole in the x-direction is probably the result of the constraint using the glue of the sample warpage during the printing phase. As in the x-direction, i.e. the major side of the specimen, the warpage is much more important than the y-direction, this could explain the difference between the residual stresses in x and y directions.

For the τ_{xy} (Fig. 18.5) it cannot be observed any significant difference among the stacking sequences, the side of the specimens, and the central and side holes. Indeed, the values of residual stress are roughly between −1 and +1 MPa in all configurations.

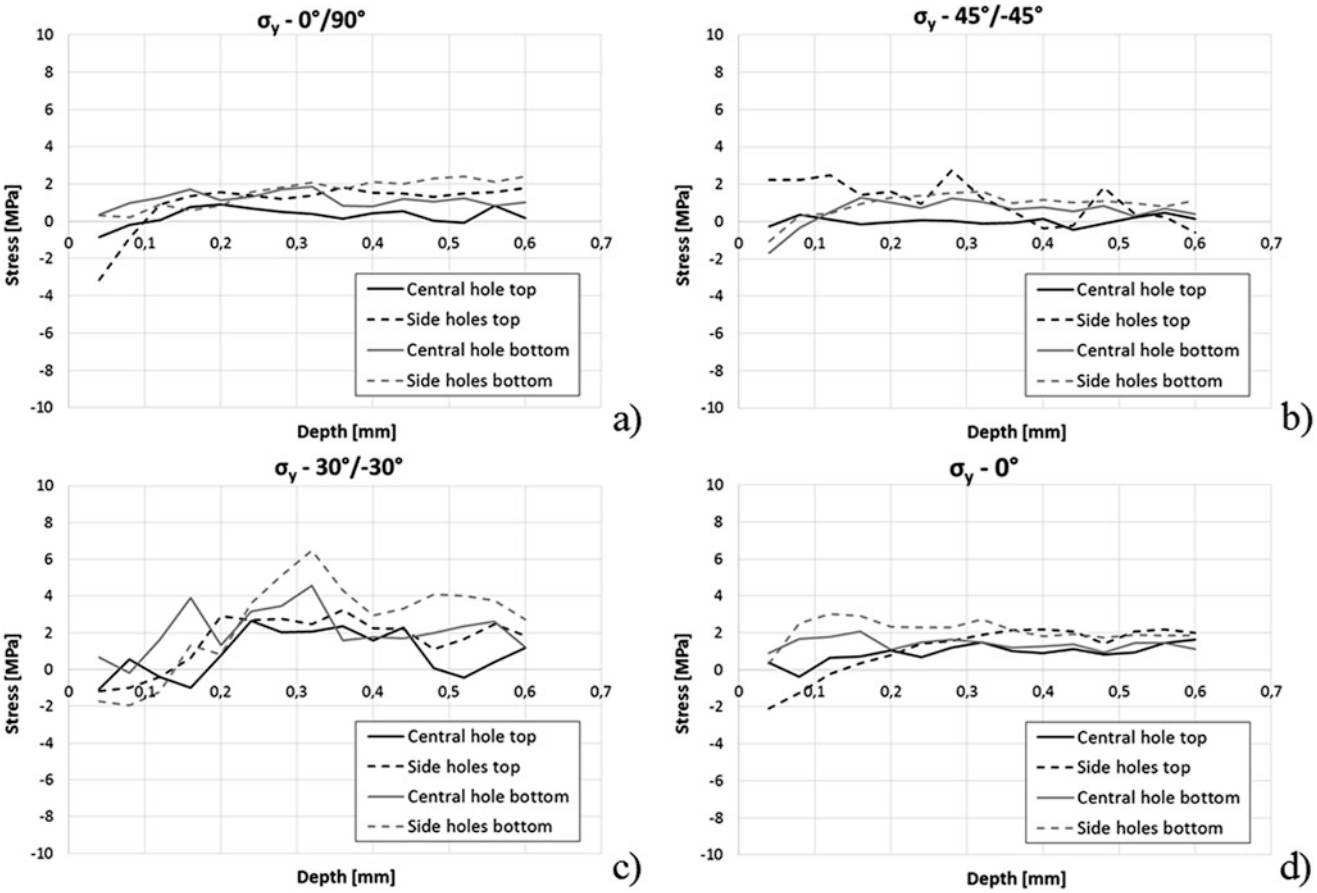

Fig. 18.4 Residual stresses in y direction for 0°/90° (**a**), 45°/−45° (**b**), 30°/−30° (**c**) and 0° (**d**) raster orientations

18.4 Conclusions

In this paper, the measure of the residual stresses in FDM printed parts has been carried out by the hole-drilling method. In order to avoid the local reinforcement of the strain gage, an optical technique, i.e. ESPI (electronic speckle pattern interferometry), is employed to measure the displacement of the surface due to the stress relaxation and, consequently, calculate the residual stresses. The aim of the work was to measure the residual stresses in several points of 3D printed parts, both on top and bottom, to verify if the constrain conditions employed during the printing produce substantial variation from a point to another. This comparison has been carried out among four stacking sequences, i.e. ±30°, ±45°, 0°/90° and 0° only. The specimens have been made of ABS and they have the dimensions of $80 \times 40 \times 7$ mm.

The results show that, whereas for σ_x and σ_y there are some differences, for τ_{xy} it cannot be observed any difference among the stacking sequences, the sides of the specimens, and the comparison between central and side holes. For σ_x and σ_y, the differences are remarkable near the surface of the specimens, i.e. until 0.2 mm, but below this depth, there are no clear differences among the studied configurations. Whereas the ±30° configuration is the worst stacking sequence because it shows the highest values of residual stresses, the ±45° should be the best configuration to have low residual stresses in the specimens.

The comparison between the residual stresses in side and central positions shows that, for the σ_x stress, the side positions has higher, in absolute value, residual stresses. On the other hand, for the σ_y stress, this difference is not clear and the different trends are almost overlapped. The difference between side and central hole is probably the result of the constrain using the glue of the sample warpage during the printing phase. As in the x-direction, i.e. the major side of the specimen, the warpage is much more important than the y-direction, this could explain the difference between the residual stresses in x and y directions. These results confirm that residual stress management in FDM part is an important problem that must be properly addressed and they show, in a clear way, that constrain the specimens avoiding the warpage increases the residual stresses in the finished part.

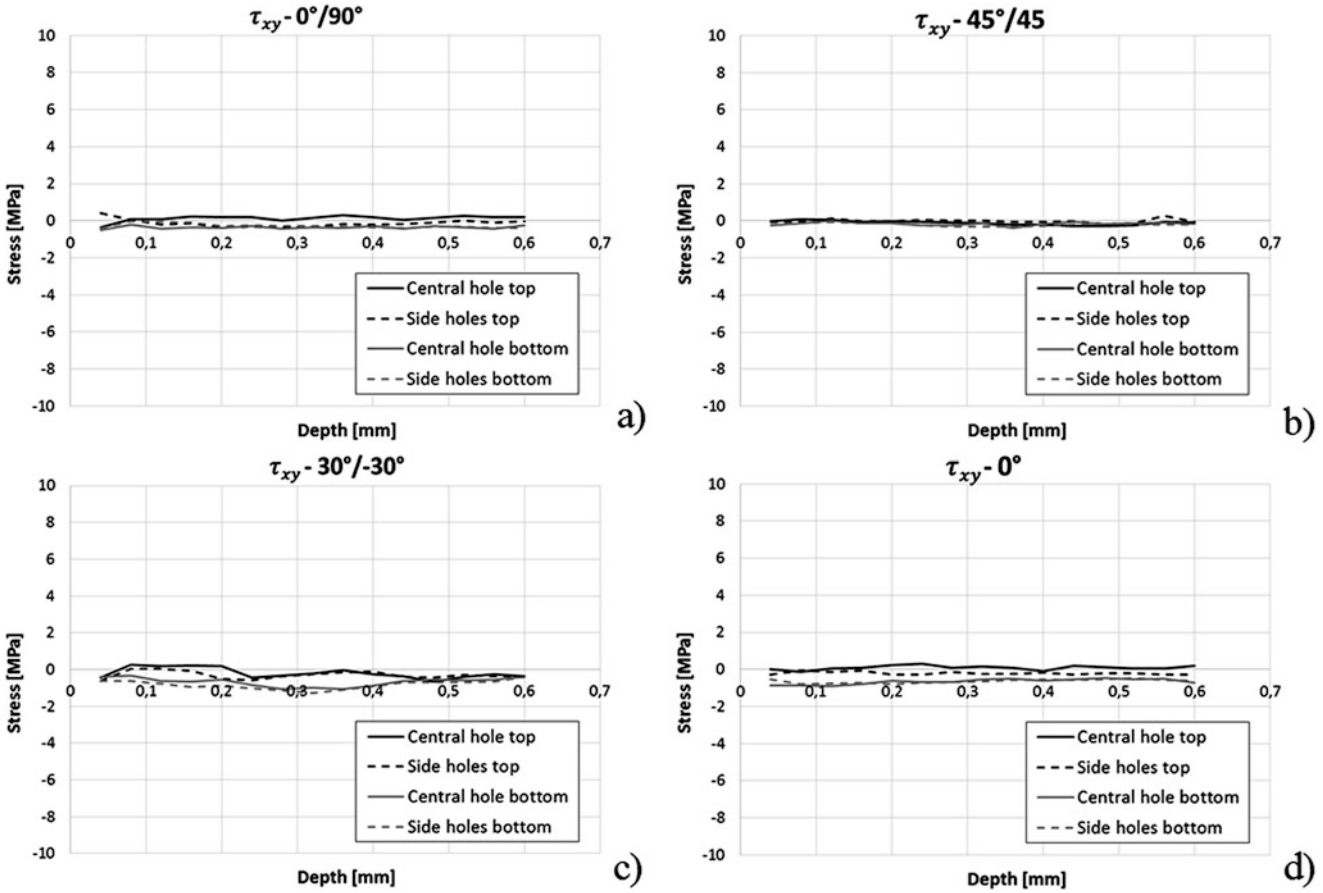

Fig. 18.5 Residual stresses in xy direction for 0°/90° (**a**), 45°/−45° (**b**), 30°/−30° (**c**) and 0° (**d**) raster orientations

Acknowledgment This research was co-funded by Fondo di Sviluppo e Coesione 2007-2013 – APQ Ricerca Regione Puglia "Regional program for Smart Specialization and Social and Environmental sustainability"– FutureInResearch.

References

1. Yan, X., Gu, P.: A review of rapid prototyping technologies and systems. Comput. Aided Des. **28**(4), 307–318 (1996)
2. Petzold, R., Zeilhofer, H.F., Kalender, W.A.: Rapid prototyping technology in medicine—basics and applications. Comput. Med. Imaging Graph. **23**(5), 277–284 (1999)
3. Chua, C.K., Chou, S.M., Wong, T.S.: A study of the state-of-the-art rapid prototyping technologies. Int. J. Adv. Manuf. Technol. **14**(2), 146–152 (1998)
4. Casavola, C., et al.: Orthotropic mechanical properties of fused deposition modelling parts described by classical laminate theory. Mater. Des. **90**, 453–458 (2016)
5. Mireles, J., et al.: Development of a fused deposition modeling system for low melting temperature metal alloys. J. Electron. Packag. **135**(1), 011008–011008 (2013)
6. Allahverdi, M., et al.: Processing of advanced electroceramic components by fused deposition technique. J. Eur. Ceram. Soc. **21**(10–11), 1485–1490 (2001)
7. Zein, I., et al.: Fused deposition modeling of novel scaffold architectures for tissue engineering applications. Biomaterials. **23**(4), 1169–1185 (2002)
8. Masood, S.H., Song, W.Q.: Development of new metal/polymer materials for rapid tooling using Fused deposition modelling. Mater. Des. **25**(7), 587–594 (2004)
9. Zhong, W., et al.: Short fiber reinforced composites for fused deposition modeling. Mater. Sci. Eng. A. **301**(2), 125–130 (2001)
10. Kantaros, A., Karalekas, D.: Fiber Bragg grating based investigation of residual strains in ABS parts fabricated by fused deposition modeling process. Mater. Des. **50**, 44–50 (2013)
11. Casavola, C., et al.: Preliminary study on residual stress in FDM parts. In: Residual Stress, Thermomechanics & Infrared Imaging, Hybrid Techniques and Inverse Problems, vol. 9, pp. 91–96. Springer International Publishing, Cham, Switzerland (2017)

12. Turnbull, A., Maxwell, A.S., Pillai, S.: Residual stress in polymers – evaluation of measurement techniques. J. Mater. Sci. **34**(3), 451–459 (1999)
13. Nau, A., et al.: Application of the hole drilling method for residual stress analyses in components made of polycarbonate. Z. Kunststofftechnik/J. Plast. Technol. **3**, 66–85 (2011)
14. Magnier, A., Nau, A., Scholtes, B.: Some aspects of the application of the hole drilling method on plastic materials. In: Conference Proceedings of the Society for Experimental Mechanics Series. (2016)
15. Casavola, C., et al.: Residual stress measurement in Fused Deposition Modelling parts. Polym. Test. **58**, 249–255 (2017)
16. Casavola, C., Campanelli, S.L., Pappalettere, C.: Preliminary investigation on distribution of residual stress generated by the selective laser melting process. J. Strain Anal. Eng. Des. **44**(1), 93–104 (2009)
17. Casavola, C., Campanelli, S.L., Pappalettere, C.: Experimental analysis of residual stresses in the selective laser melting process. Society for Experimental Mechanics – 11th International Congress and Exhibition on Experimental and Applied Mechanics 2008, 3, pp. 1479–1486, 2008
18. Zhang, Y., Chou, Y.: Three-dimensional finite element analysis simulations of the fused deposition modelling process. Proc. Inst. Mech. Eng. B J. Eng. Manuf. **220**(10), 1663–1671 (2006)
19. Kujawinska, M.: Use of phase-stepping automatic fringe analysis in moire interferometry. Appl. Opt. **26**(22), 4712–4714 (1987)
20. Ghiglia, D.C., Pritt, M.D.: Two-dimensional phase unwrapping: Theory, algorithms, and software, vol. 4. Wiley, New York (1998)